

- 10) V. N. Ingal and E. A. Beliaevskaya: *J. Phys. D* **28** (1995) 2314.
- 11) D. Chapman, W. Thomlinson, R. E. Johnston, D. Washburn, E. Pisano, N. Gmür, Z. Zhong, R. Menk, F. Arfelli and D. Sayers: *Phys. Med. Biol.* **42** (1997) 2015.
- 12) A. Snigirev, I. Snigireva, V. Kohn, S. Kuznetsov and I. Schelokov: *Rev. Sci. Instrum.* **66** (1995) 5486.
- 13) K. A. Nugent, T. E. Gureyev, D. F. Cookson, D. Paganin and Z. Barnea: *Phys. Rev. Lett.* **77** (1996) 2961.
- 14) S. W. Wilkins, T. E. Gureyev, D. Gao, A. Pogany and A. W. Stevenson: *Nature* **384** (1996) 335.
- 15) P. Cloetens, W. Ludwig, J. Baruchel, D. Van Dyck, J. Van Landuyt, J. P. Guigay and M. Schlenker: *Appl. Phys. Lett.* **75** (1999) 2912.
- 16) F. A. Dilmanian, Z. Zhong, B. Ren, X. Y. Wu, L. D. Chapman, I. Orion and W. C. Thomlinson: *Phys. Med. Biol.* **45** (2000) 933.
- 17) I. Koyama, Y. Hamaishi and A. Momose: *AIP Conf. Proc.* **705** (2004) 1283.
- 18) A. Maksimenko, M. Ando, H. Sugiyama and T. Yuasa: *Appl. Phys. Lett.* **86** (2005) 124105.
- 19) I. Koyama, A. Momose, J. Wu, Thet Thet Lwin and T. Takeda: *Jpn. J. Appl. Phys.* **44** (2005) 8219.
- 20) Konica Minolta Technol. Rep. **2** (2005) 30 [in Japanese].
- 21) C. David, B. Nöhammer, H. H. Solak and E. Ziegler: *Appl. Phys. Lett.* **81** (2002) 3287.
- 22) A. Momose, S. Kawamoto, I. Koyama, Y. Hamaishi, K. Takai and Y. Suzuki: *Jpn. J. Appl. Phys.* **42** (2003) L866.
- 23) A. Momose, S. Kawamoto, I. Koyama and Y. Suzuki: *Proc. SPIE* **5535** (2004) 352.
- 24) T. Weitkamp, B. Nöhammer, A. Diaz, C. David and E. Ziegler: *Appl. Phys. Lett.* **86** (2005) 054101.
- 25) T. Weitkamp, A. Daiz, C. David, F. Pfeiffer, M. Stampanoni, P. Cloetens and E. Ziegler: *Opt. Express* **13** (2005) 6296.
- 26) S. Yokozeki and T. Suzuki: *Appl. Opt.* **10** (1971) 1575.
- 27) A. W. Lohmann and D. E. Silva: *Opt. Commun.* **2** (1971) 413.
- 28) A. Momose and S. Kawamoto: *Jpn. J. Appl. Phys.* **45** (2006) 314.
- 29) M. Matsumoto, K. Takiguchi, M. Tanaka, Y. Hunabiki, H. Takeda, A. Momose, Y. Utsumi and T. Hattori: *High Aspect Ratio Micro Structure Technology Workshop, 2005*, p. 22.
- 30) P. Cloetens, J. P. Guigay, C. De Martino, J. Baruchel and M. Schlenker: *Opt. Lett.* **22** (1997) 1059.
- 31) H. F. Talbot: *Philos. Mag.* **9** (1836) 401.
- 32) J. P. Guigay: *Opt. Acta* **18** (1971) 677.
- 33) M. Born and E. Wolf: *Principle of Optics* (Pergamon Press, Oxford, 1980) p. 508.
- 34) J. H. Bruning, D. R. Herriott, J. E. Gallagher, D. P. Rosenfeld, A. D. White and D. J. Brangaccio: *Appl. Opt.* **13** (1974) 2693.
- 35) K. A. Stetson and W. R. Brohinsky: *Appl. Opt.* **24** (1985) 3631.
- 36) J. M. Huntley: *Appl. Opt.* **28** (1989) 3268.
- 37) G. W. Faris and R. L. Byer: *Appl. Opt.* **27** (1988) 5202.
- 38) A. Momose, T. Takeda, Y. Itai and K. Hirano: *Nat. Med.* **2** (1996) 473.
- 39) A. Momose, T. Takeda and Y. Itai: unpublished.
- 40) K. Paturski: *Progress in Optics* (Elsevier, Amsterdam, 1989) Vol. 27.
- 41) W. Yashiro and A. Momose: in preparation.

# Biomedical Imaging by Talbot-Type X-Ray Phase Tomography

Atsushi Momose<sup>a</sup>, Wataru Yashiro<sup>a</sup>, Masafumi Moritake<sup>a</sup>, Yoshihiro Takeda<sup>b</sup>,  
Kentaro Uesugi<sup>c</sup>, Akihisa Takeuchi<sup>c</sup>, Yoshio Suzuki<sup>c</sup>, Makoto Tanaka<sup>d</sup>, and Tadashi Hattori<sup>d</sup>

<sup>a</sup>Department of Advanced Materials Science, Graduate School of Frontier Sciences, The  
University of Tokyo, 5-1-5 Kashiwanoha, Kashiwa, Chiba 277-8651, Japan;

<sup>b</sup>Graduate School of Pure and Applied Sciences, University of Tsukuba, 1-1-1 Tennodai,  
Tsukuba, Ibaraki 305-8573, Japan;

<sup>c</sup>SPring-8/JASRI, 1-1-1, Kouto, Sayo, Hyogo 679-5198 Japan;

<sup>d</sup>Laboratory of Advanced Science and Technology for Industry, University of Hyogo, 3-1-2  
Kouto, Kamigori, Hyogo 678-1205, Japan

## ABSTRACT

An X-ray Talbot interferometer for X-ray phase imaging and tomography was constructed using an amplitude grating of a gold pattern 8  $\mu\text{m}$  in pitch and 30  $\mu\text{m}$  in height developed by X-ray lithography and gold electroplating. The effective area of the grating was 20 mm  $\times$  20 mm, and was fully illuminated by synchrotron radiation at beamline 20XU, SPring-8, Japan. Almost whole body of a fish 3 cm in length was observed by phase tomography. Resulting images obtained with 0.07 nm and 0.045 nm X-rays revealed organs with bones in the same view successfully. A preliminary result of the combination with an X-ray imaging microscope is also presented, which was attempted to attain a higher spatial resolution. Finally, prospects of the compatibility with a conventional X-ray generator are discussed for practical applications such as clinical diagnoses.

**Keywords:** Phase, Imaging, Tomography, Talbot effect, Talbot interferometer, Grating

## 1. INTRODUCTION

Recently, phase differential X-ray interferometry using X-ray transmission gratings has been attracting attentions as a novel phase-sensitive X-ray imaging method.<sup>1-4</sup> A contrast corresponding to the wavefront inclination caused by the X-ray refraction at a sample can be sensed. Its principle is the same as that of optical Talbot interferometry<sup>5,6</sup> that aligns two transmission gratings on an optical axis. The first grating causes the fractional Talbot effect; that is, a periodic intensity pattern, which we call as a 'self-image' in this paper, is formed at a specific distance from the grating determined by the pitch of the gratings and X-ray wavelength. When a phase object is placed in the beam path, the refraction at the sample reflects on the deformation of the self-image. The Talbot interferometer generate a moiré pattern by placing an amplitude grating, whose pitch is almost the same as the average period of the self-image, at the position of the self-image, as shown in Fig. 1(a).

Not only the generation of a phase-sensitive contrast but also quantitative measurement of the wavefront inclination, in other words a differential phase map, can be performed with an X-ray Talbot interferometer, allowing X-ray phase tomography. In this paper, we report a biological imaging result obtained using synchrotron radiation, including technical progress made since the previous report.<sup>7</sup> Because of using grating optics, X-ray Talbot interferometry has an attractive advantage that cone-beam and/or polychromatic X-rays are available. It is therefore possible to combine an X-ray Talbot interferometer with an X-ray imaging microscope. A preliminary experiment of Talbot-type phase-sensitive X-ray microscopy is also presented. Finally, the compatibility of X-ray Talbot interferometry with a conventional X-ray source for practical applications outside synchrotron facilities are discussed.

---

A.M.: E-mail: momose@exp.t.u-tokyo.ac.jp

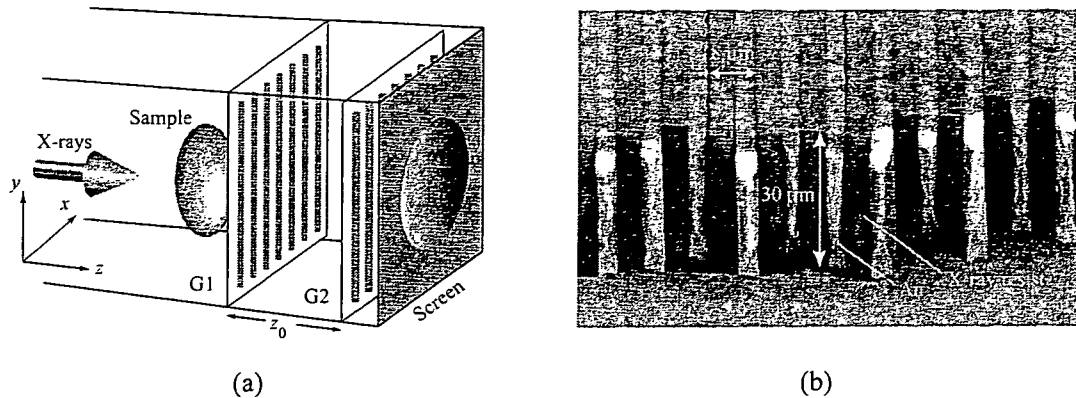


Figure 1. Configuration of X-ray Talbot interferometer (a), where phase grating (G1) and amplitude grating (G2), whose SEM image is shown in (b), are aligned in line along X-ray axis.

## 2. METHOD

### 2.1. X-ray Gratings

An X-ray absorption grating is the key optical element in the successful operation of an X-ray Talbot interferometer. The visibility of moiré fringes is determined by the thickness of the grating pattern. We selected gold as a material of the pattern because of its high absorption coefficient and fabrication convenience. Nevertheless, a thickness of several tens of microns is required to block X-rays sufficiently. For instance, roughly 10  $\mu\text{m}$  is needed at 20 keV, 30  $\mu\text{m}$  at 30 keV, and 60  $\mu\text{m}$  at 40 keV. On the other hand, the pitch of the grating should be comparable to the spatial coherent length of incident X-rays, which is in general of the order of microns. It is not straightforward to fabricate such a pattern of a high aspect ratio with conventional lithographic techniques. We have therefore attempted at fabricating X-ray amplitude gratings by X-ray lithography and gold electroplating.

The synchrotron radiation beamline 11 of NewSUBARU, Japan, which is dedicated to lithographic galvanofarming abformung (LIGA) fabrication, was used. A 30  $\mu\text{m}$  X-ray resist film (MAX001, Nagase ChemteX) was spin-coated on a 200- $\mu\text{m}$  Si wafer with a 0.25- $\mu\text{m}$  Ti layer, and then a 4- $\mu\text{m}$  L&S resist pattern (8  $\mu\text{m}$  pitch) was fabricated by X-ray exposure. Gold lines were formed by electroplating between resist lines, which were left after the electroplating to support the gold lines (Fig. 1(b)). The effect of absorption by the X-ray resist is negligible. The height of the gold lines was nearly 30  $\mu\text{m}$ , and the effective area of the grating was 20  $\times$  20  $\text{mm}^2$ .<sup>8</sup>

### 2.2. Tomographic Reconstruction

An X-ray Talbot interferometer consists of a phase grating (G1), an amplitude grating (G2) and an image detector. The spacing between the gratings is set so that the fractional Talbot effect by G1 occurs at the position of G2; that is, a self-image with a period corresponding to the pitch of G1 is formed on G2. When a phase object is placed in front of G1 or between G1 and G2, the self-image is deformed owing to the X-ray refraction at the object. When the pitch of G2 is almost the same as the pitch of the self-image, a moiré pattern is observed by an image detector placed just behind G2.

With plane-wave illumination, the self-image  $I(x, y, z)$  formed by a grating is given by

$$I(x, y, z) = \left| \sum_n a_n \exp\left(-\pi i \lambda z \frac{n^2}{d^2}\right) \exp\left(2\pi i \frac{nx}{d}\right) \right|^2 \quad (1)$$

under a paraxial approximation, where  $d$ ,  $\lambda$ , and  $a_n$  are the pitch of the grating, X-ray wavelength, and the coefficient of the Fourier series expansion of the complex transmission function of the grating, respectively. Here, the X-ray optical axis is parallel to the  $z$  axis, and the line pattern of the gratings is parallel to the  $y$  axis.

When a phase object that causes a phase shift  $\Phi(x, y)$  is placed close to G1 ( $z = 0$ ), the phase of the  $n$ -th order diffraction by G1 is given by

$$\Phi\left(x - \frac{n\lambda z}{d}, y\right) \approx \Phi(x, y) - \frac{n\lambda z}{d} \frac{\partial \Phi(x, y)}{\partial x} \quad (2)$$

with geometrical consideration. Equation (1) is therefore rewritten as

$$\begin{aligned} I(x, y, z) &= \left| \sum_n a_n \exp\left(-\pi i \lambda z \frac{n^2}{d^2}\right) \exp\left[i\left\{2\pi \frac{nx}{d} + \Phi\left(x - \frac{n\lambda z}{d}, y\right)\right\}\right] \right|^2, \\ &\approx \sum_n b_n(z) \exp\left[2\pi i \frac{n}{d}(x - z\varphi(x, y))\right], \end{aligned} \quad (3)$$

where

$$\varphi(x, y) = \frac{\lambda}{2\pi} \frac{\partial \Phi(x, y)}{\partial x}, \quad (4)$$

and  $b_n(z)$  is given by

$$b_n(z) = \sum_{n'} \beta_{n+n'} \beta_{n'}^*, \quad \beta_n \equiv a_n \exp\left(-\pi i \lambda z \frac{n^2}{d^2}\right). \quad (5)$$

It is known that 100% visibility is attained in principle when a self-image is observed at

$$z = d^2/2\lambda \quad (6)$$

with a  $\pi/2$  phase grating.<sup>9</sup>

Giving the transmission function of G2, which has a pitch the same as the average period of  $I(x, y, z)$ , with

$$T(x, y) = \sum_n t_n \exp\left(2\pi i \frac{nx}{d}\right), \quad (7)$$

a moiré pattern

$$\begin{aligned} M(x, y, z) &= I(x, y, z) \times T(x + \chi, y) \\ &= \sum_n b_n(z) t_n \exp\left\{2\pi i \frac{n}{d}(z\varphi(x, y) + \chi)\right\} \end{aligned} \quad (8)$$

is observed.  $\chi$  is the displacement of G2 in the  $x$  direction, and this freedom can be used for the quantitative measurement of  $\varphi(x, y)$  by the fringe scanning method; that is,

$$2\pi \frac{z}{d} \varphi(x, y) \approx \arg \left[ \sum_k^M M_k(x, y, z) \exp\left(-2\pi i \frac{k}{M}\right) \right], \quad (9)$$

where  $M_k(x, y, z)$  is the moiré pattern when  $\chi = kd/M$  ( $k = 1, 2, \dots, M$ ). Strictly, higher orders in eq. (8) cause error in the determination of  $\varphi(x, y)$  with eq. (9). If a sufficiently large number is selected for  $M$ , such an error can be reduced.<sup>4, 7, 10</sup>

The input data of phase tomography is normally  $\Phi(x, y, \theta)$ , which is the projection of the refractive index difference  $\delta$ ; that is,

$$\Phi(x, y, \theta) = \frac{2\pi}{\lambda} \int \delta(X, y, Z) dz, \quad (10)$$

where  $(X, y, Z)$  is the coordinate fixed with the object, and  $\theta$  is the angle between the  $x$  and  $X$  axes. In the present case, we measure  $\varphi(x, y)$  that satisfies

$$\varphi(x, y, \theta) = \int \frac{\partial \delta(X, y, Z)}{\partial x} dz. \quad (11)$$

In order to follow the process based on eq. (10), one may calculate  $\Phi(x, y, \theta)$  by integrating  $\varphi(x, y, \theta)$  although stripe artifact caused by noise accumulation appears occasionally in a resultant image corresponding to  $\Phi(x, y, \theta)$ . However, it is also possible to reconstruct  $\delta(X, y, Z)$  directly from  $\varphi(x, y, \theta)$  as below.<sup>11</sup>

In tomographic algorithm,

$$\delta(X, y, Z) = \int_0^\pi \int_{-\infty}^{\infty} P(\omega, y, \theta) \exp[2\pi i \omega (X \cos \theta - Z \sin \theta)] |\omega| d\omega d\theta \quad (12)$$

is calculated, where  $P(\omega, y, \theta)$  is the Fourier transform of experimental data (that is,  $\Phi(x, y, \theta)\lambda/2\pi$  in this case). Here, it should be noted that the Fourier transform of  $\varphi(x, y, \theta)$ ,  $A(\omega, y, \theta)$ , is given using  $P(\omega, y, \theta)$  by

$$A(\omega, y, \theta) = 2\pi i \omega P(\omega, y, \theta). \quad (13)$$

Then, eq. (12) is rewritten as

$$\delta(X, y, Z) = \frac{1}{2\pi i} \int_0^\pi \int_{-\infty}^{\infty} A(\omega, y, \theta) \exp[2\pi i \omega (X \cos \theta - Z \sin \theta)] \text{sgn}(\omega) d\omega d\theta, \quad (14)$$

where  $\text{sgn}(\omega)$  is the sign function

$$\text{sgn}(\omega) = \begin{cases} 1 & \omega > 0, \\ -1 & \omega < 0. \end{cases} \quad (15)$$

Thus,  $\varphi(x, y, \theta)$  can be used for the input data of filtered-backprojection method with  $\text{sgn}(\omega)/2\pi i$  as a filter function. Phase tomograms mapping the  $\delta$  presented in the next Section were reconstructed with this approach.

### 3. BIOLOGICAL IMAGING WITH SYNCHROTRON RADIATION

An X-ray Talbot interferometer was constructed with a grating described above first at the beamline 20XU of SPring-8, Japan, where undulator radiation 245 m downstream from the source was available. The fundamental performance of the X-ray Talbot interferometer was reported previously<sup>4</sup>; the visibility of the generated moiré pattern was about 80% with the X-ray wavelength at 0.065 nm, and even at 0.03 nm, over 30% visibility was attained and tomographic imaging could be carried out.

A demonstration described in this paper was carried out at the beamline 20B2 of SPring-8, where a wide beam was available from a bending section. The effective area of the gratings (20 mm × 20 mm) was entirely illuminated by X-rays, and almost whole body imaging was performed for a fish (*Hasemanina nana*) 3 cm in length. The fish was put in a cell filled with formalin, and placed just in front of the phase grating. The fish was rotated about the  $y$  axis with a step of 0.36° over 180°.  $\varphi(x, y, \theta)$  was measured at every angular position of the sample rotation by the fringe scanning method with a  $d/5$  step of displacement of the amplitude grating. Moiré patterns were recorded with a CCD camera (C4742-95HR, Hamamatsu Photonics) lens-coupled with a phosphor screen. Its effective pixel size was 11.8  $\mu\text{m}$  × 11.8  $\mu\text{m}$ . The exposure time for obtaining a moiré pattern was 8.2 s.

Figures 2 and 3 show reconstructed tomograms measured using 0.07-nm X-rays. Although some line artifacts arose from the surface and bone, organ structures were clearly revealed with bones in the same view. The line artifacts appear always at the region where the spatial change in the refractive index is prominent, in other words, where the beam deflection is comparatively large. This implies that  $\varphi(x, y, \theta)$  is not determined correctly at clear structural boundaries within the assumption used in the formulation described above. In order to reduce the artifact, we need to reconsider eq. (2) or eq. (11); that is, the propagation of wavefront from the sample to the detector should be dealt with the theory of wave optics in the future.

Figure 4 shows the visibility of the moiré fringes observed at the beamline 20B2. Although the visibility decreased with increasing X-ray energy, the X-ray Talbot interferometer exhibited moiré fringes with a visibility sufficient for phase imaging at 0.04 nm. The fish sample was also observed with 0.045-nm X-rays, and images almost comparable to those by 0.07 nm X-rays were obtained, as shown in Fig. 5.

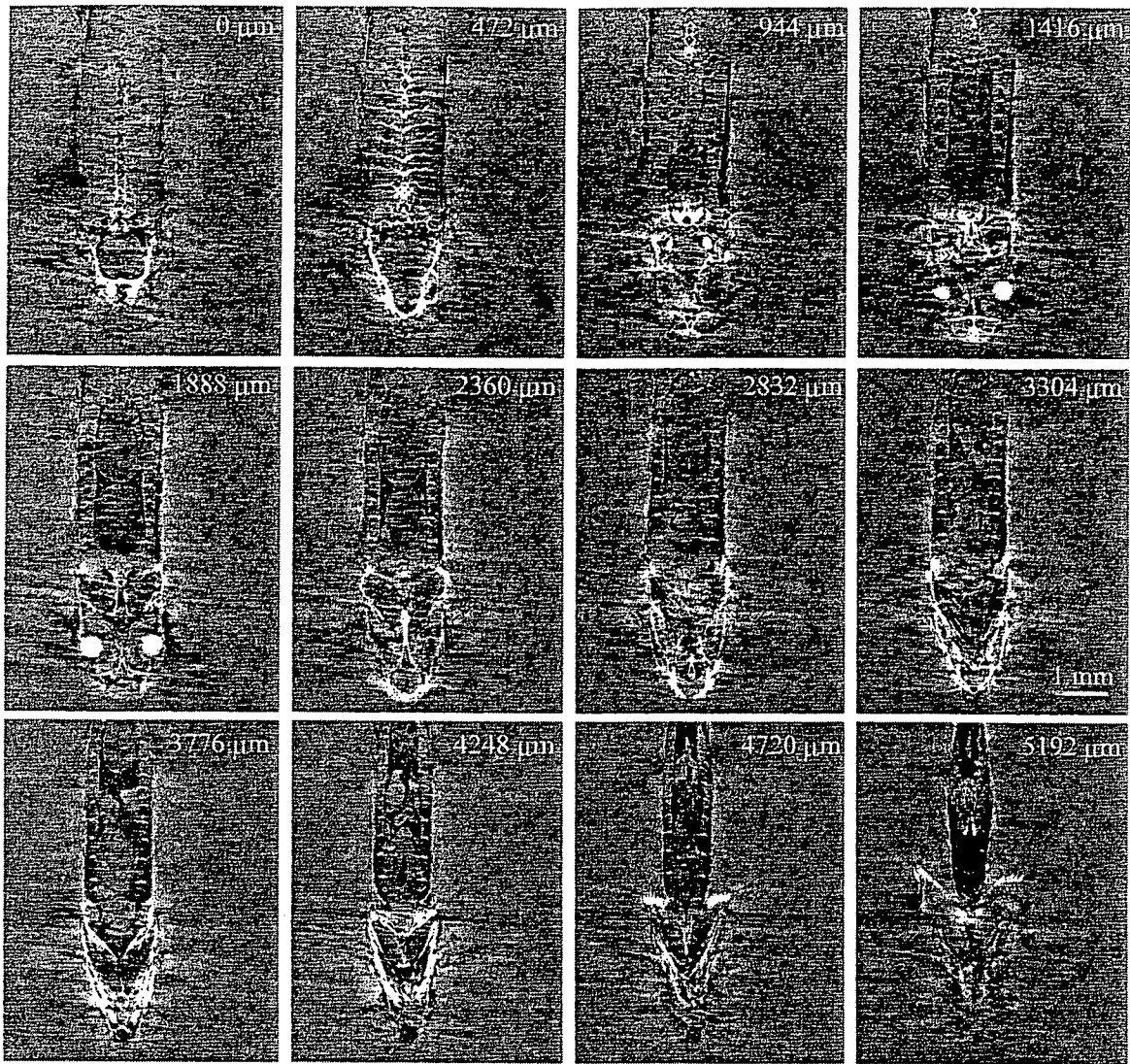


Figure 2. Phase tomograms (coronal views) of a fish (*Hasemania nana*) 3 cm in length from the back to the stomach. The relative positions of the tomograms are shown. X-ray wavelength was 0.07 nm.

## 4. PROSPECTS

### 4.1. Combination with an X-ray imaging microscope

The spatial resolution of X-ray phase imaging by Talbot interferometry is limited by the pitch of the grating. One approach for improving the spatial resolution is the reduction of the pitch. Another approach is the combination with X-ray imaging microscopy. X-ray imaging microscopes, which use focusing optics such as Fresnel zone plates, have been intensively developed using synchrotron X-rays. Because a Talbot interferometer functions for a spherical-wave X-rays because of using grating optics, the combination shown in Fig. 6 is feasible.

A preliminary experiment was carried out at the beamline 20XU of SPring-8, using a zone plate (ZP100-320-16, Xradia) whose outermost zone width, diameter, and gold-pattern thickness were 100 nm, 320  $\mu\text{m}$ , and 1.6  $\mu\text{m}$ , respectively. A sample was placed 339 mm upstream of the zone plate and a CCD-based X-ray image detector, whose effective pixel size was 3.14  $\mu\text{m}$ , was set at the position 5.96 m from the zone plate. The focal length of the zone plate was 320 mm and the magnification of the system was 17.6. An amplitude grating 8

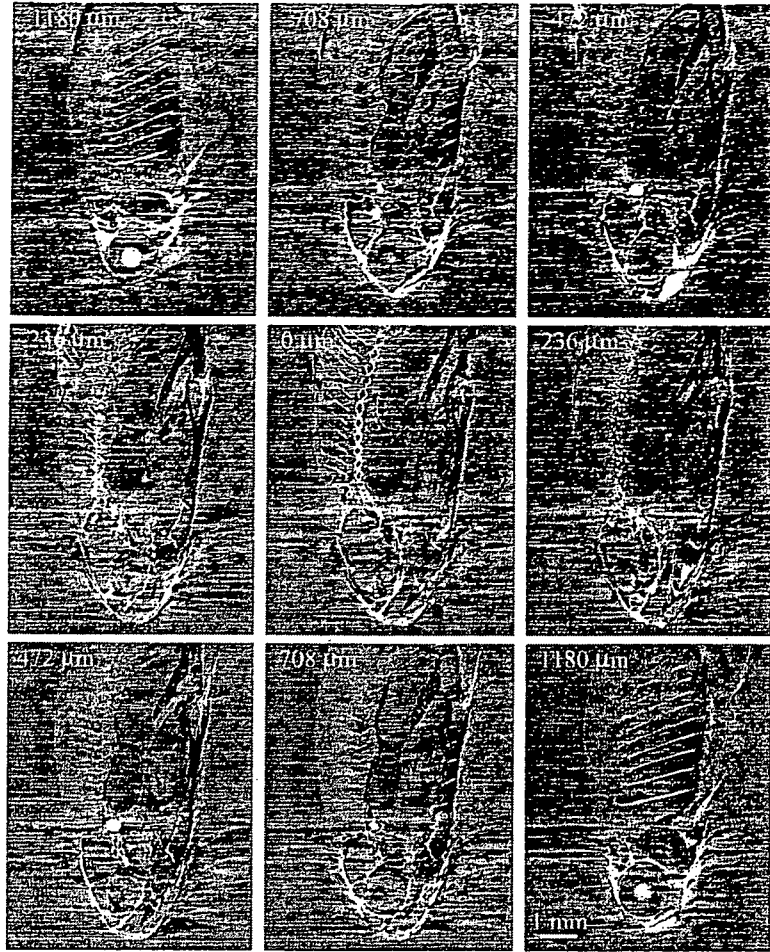


Figure 3. Phase tomograms (sagittal views) of a fish (*Hasemania nana*) 3 cm in length. The relative positions of the tomograms are shown. X-ray wavelength was 0.07 nm.

$\mu\text{m}$  in pitch was placed just in front of the image detector and the phase grating  $8 \mu\text{m}$  in pitch was set 339 mm upstream of the amplitude grating. The distance was calculated by

$$z = \left( \frac{1}{z_0} - \frac{1}{r} \right)^{-1}, \quad (16)$$

where  $z_0$  is the distance in the case of plane-wave illumination given by eq. (6), and  $r$  is the distance from the focal point to the phase grating.

Figure 7(a) shows a resultant image obtained using 0.1 nm X-rays. We used a set of gratings used in the plane-wave experiment described above. Moiré fringes therefore appeared because the period of the self-image was enlarged to  $d(r+z)/r$  which was mismatched with the pitch of the amplitude grating. The fringes were not crucial because their effect could be removed during the calculation of a differential phase map (Fig. 7(b)) by the fringe scanning method. A sample consisting of polystyrene spheres was used for this demonstration, which suggests that an X-ray Talbot interferometer, in other words an X-ray phase-sensitive detector, can be used to adapt a phase-contrast mode to X-ray imaging microscopes.

#### 4.2. Combination with a compact X-ray source

The high sensitivity of X-ray phase imaging is attractive from a medical point of view. For practical applications, however, it is important to develop imaging systems outside huge synchrotron facilities. As mentioned, an X-ray

Talbot interferometer functions with spherical-wave (cone-beam) X-rays. Therefore, laboratory (or hospital) X-ray generators are available, provided that the spatial coherence is assured to be as high as needed for the operation of an X-ray Talbot interferometer. As discussed in the previous paper,<sup>4</sup> the spatial coherence length  $L$  given by

$$L = \frac{\lambda R}{2\pi\sigma_x}, \quad (17)$$

at the distance  $R$  from a source with a Gaussian intensity distribution  $\exp(-x^2/2\sigma_x^2)$  should satisfy

$$L > d/3 \quad (18)$$

when a  $\pi/2$  phase grating is used. We are now developing a phase grating of a pitch of  $4.5 \mu\text{m}$  for a cone-beam X-ray Talbot interferometer, and in that case  $\sigma_x < 4.2 \mu\text{m}$  ( $10 \mu\text{m}$  FWHM) is needed when  $R = 1 \text{ m}$  and  $\lambda = 0.04 \text{ nm}$ . Because no restriction is put with respect to the spatial coherence in the  $y$  direction, a line focus is strictly available if the thickness of the line is smaller than the requirement.

Such an X-ray source is commercially available, but its flux is not high. Applications to non-destructive

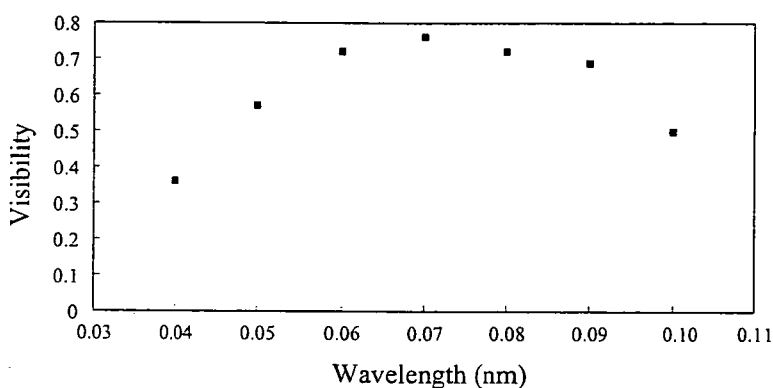


Figure 4. Visibility of moiré fringes generated by the X-ray Talbot interferometer as a function of X-ray wavelength.

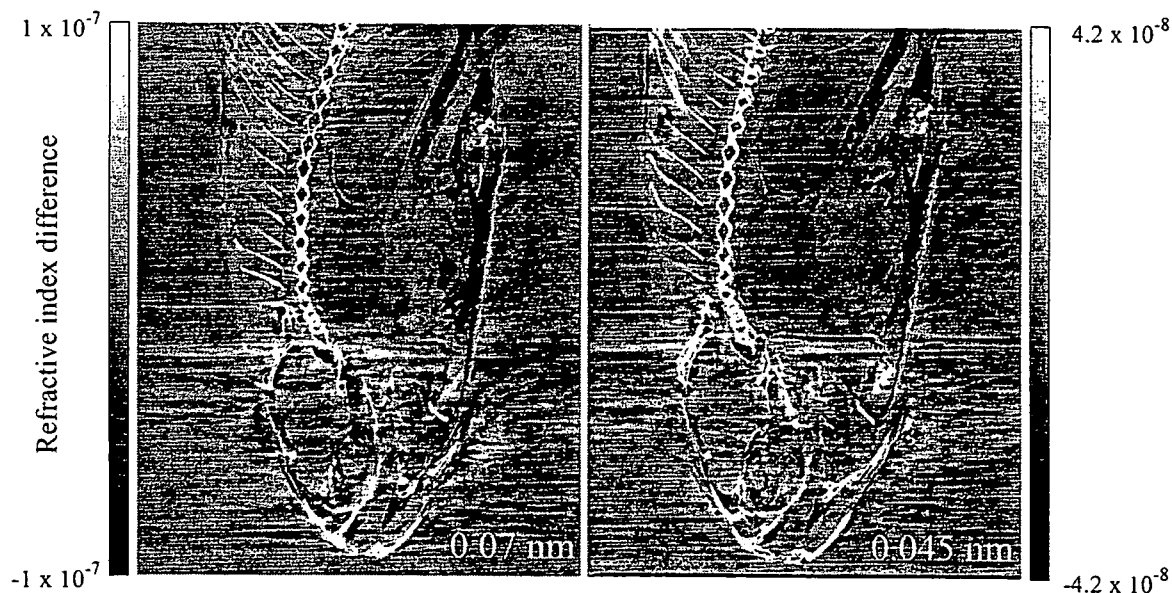


Figure 5. Comparison of the tomograms of the fish obtained with 0.07 nm and 0.045 nm X-rays.



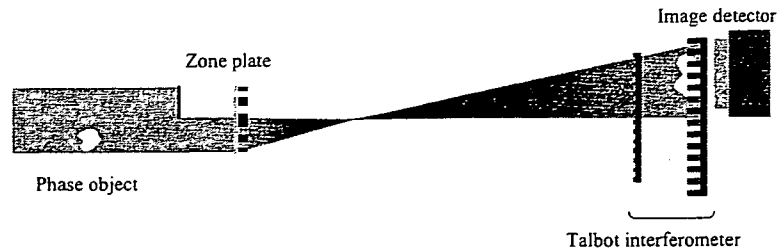


Figure 6. Phase-sensitive X-ray microscope attained by combining X-ray Talbot interferometer with X-ray imaging microscope.

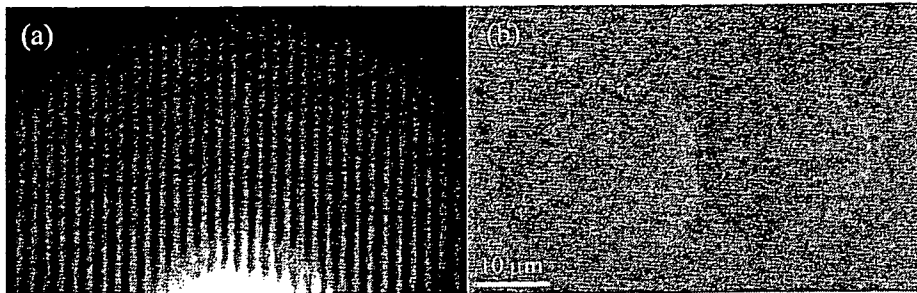


Figure 7. Result of Talbot-type X-ray imaging microscope; (a) moiré image and (b) differential phase map of polystyrene spheres.

observation that allow a long-time exposure may be feasible with such a source. However, radiologists do not accept a long-time exposure for clinical use. The development of high-flux microfocuss X-ray generator is therefore required for practical application of X-ray Talbot interferometry.

Recently, X-ray Talbot-Lau interferometry has been demonstrated as an alternative approach, which employs a one-dimensional array of X-ray sources.<sup>12</sup> The size of the individual X-ray source corresponds to that required in X-ray Talbot interferometry. The period of the array  $d_0$  is determined so that the self-images (period  $d$ ) formed by the individual sources overlap with a displacement equal to the multiple of  $d$ ; that is,

$$d_0 = \frac{R}{z} md, \quad (m = 1, 2, \dots) \quad (19)$$

where  $z$  is the distance from the grating to the self-image. It should be noted that coherency between individual sources is not needed. Practically the array is realized by using a multi-slit in combination with an X-ray source of a comparatively large focus. This approach allow us to use a conventional high-power X-ray source, and therefore X-ray Talbot-Lau interferometry is promising for clinical applications. (Because the use of the multi-slit implies the increase of the size of the entire source, one needs to compensate the decrease in the spatial resolution to some extent.)

However, it should be continued to develop thicker amplitude gratings so that higher-energy X-rays can be used. Mammography is normally performed by using X-rays of comparatively low energies from a Mo source. When X-ray phase information is available, we no longer need to be persistent to the energy region because a sufficient contrast can be obtained in the higher energy region where the reduction in X-ray dose is attained. As mentioned, our amplitude grating has a pattern 30  $\mu\text{m}$  in height, and it functioned with X-rays up to 30 keV. Stacking such gratings may be a possible approach for attaining effectively a taller pattern; up to 40 keV will be used by stacking two.

A normal X-ray generator emits characteristic X-rays and continuous X-rays. Although characteristic X-rays are favorable for the operation of the Talbot interferometer, few target materials are available for generating characteristic X-rays in the energy range of 30-40 keV. Therefore, we need an option of using continuous X-rays.

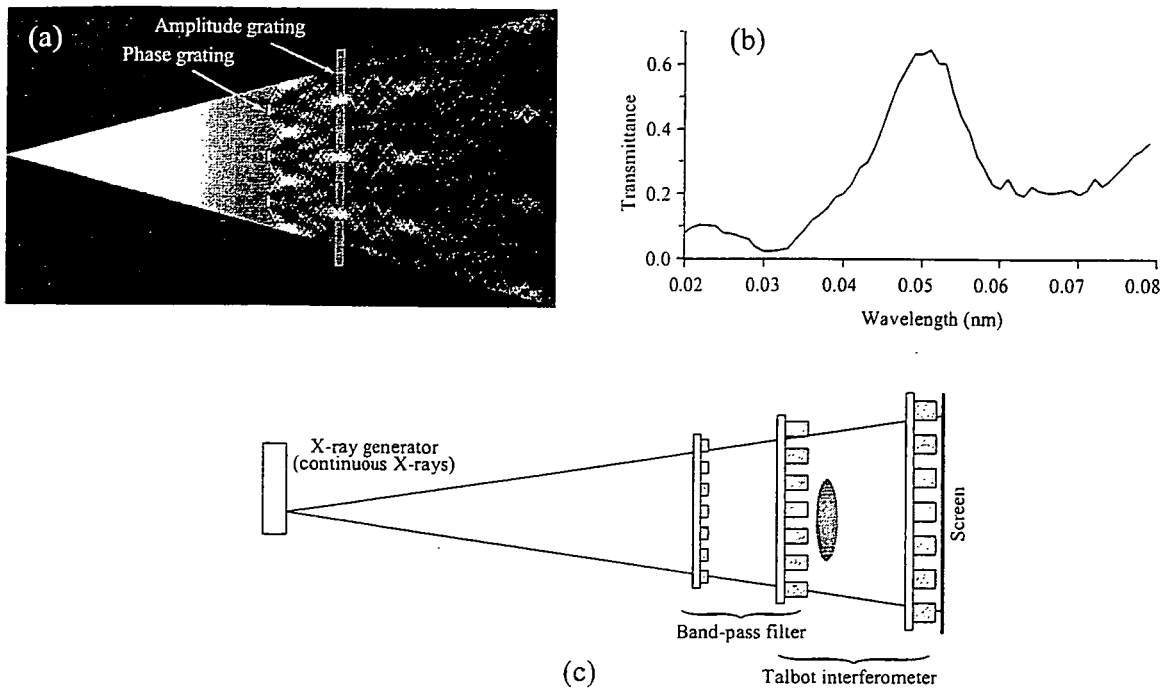


Figure 8. Band-pass filtering by fractional Talbot effect; (a) simulation of the X-ray intensity downstream of a  $\pi$  phase grating, and (b) spectral X-ray transmittance in the case that an amplitude grating is placed as shown in (a). (c) is an imaging setup with a continuous X-ray source and the band-pass filtering.

A Talbot interferometer functions with X-rays of a broad energy band because of using grating optics. In the previous paper,<sup>4</sup> it was estimated that a band width  $\Delta E/E < 1/8$  is available for X-ray Talbot interferometry. Monochromatization using a crystal, as normally adopted, is not suitable because the X-ray intensity would be reduced drastically.

Band-pass filtering for such a band width is attained by using the fractional Talbot effect. Figure 8(a) shows an intensity pattern downstream of a  $\pi$  phase grating of a 3:1 duty ratio. Remarkable concentration of the X-ray intensity is found at various positions from the grating. An amplitude grating is placed in one of such positions so that the concentrated X-rays can pass between the lines of the grating pattern. Here, it should be noted that the feature of Fig. 8(a) varies depending on X-ray energy. Therefore, this setting has a function of band-pass filtering. Figure 8(b) is a simulated spectral transmittance; thus,  $\Delta E/E \sim 1/2$  is achieved. Because the spectrum of continuous X-rays has a cut-off on the high-energy side owing to the source operation condition and/or a filter and a reduction on the low-energy side owing to absorption by air and a filter, it will be able to tailor a spectrum suitable for an X-ray Talbot interferometer. As shown in Fig. 8(c), a third grating (amplitude type) is placed at the position that the fractional Talbot effect by the second grating occurs. Thus, the set of the first and second gratings functions as a band-pass filter and the set of the second and third gratings functions as a Talbot interferometer. In this case, a sample should be downstream of the second grating. Although it is possible to place the sample upstream of the second grating, one needs to accept some performance degradation of the band-pass filtering.

## 5. CONCLUSION

Phase tomography with an X-ray Talbot interferometer was performed for almost whole body three-dimensional imaging of a fish 3 cm in length. An amplitude grating of a gold pattern  $8 \mu\text{m}$  pitch and  $30 \mu\text{m}$  thick fabricated by X-ray lithography and electroplating was used to construct the Talbot interferometer. An X-ray Talbot interferometer has advantage that spherical-wave and/or polychromatic X-rays are available. A preliminary

operation of a phase-sensitive X-ray microscope by combining an X-ray Talbot interferometer with a normal X-ray imaging microscope was reported. Practical applications of X-ray Talbot interferometry with a conventional X-ray source is promising.

## ACKNOWLEDGMENTS

The experiment using synchrotron radiation was performed under the approval of the SPring-8 committee 2006A1237-NM-np and 2006A1377. This study was financially supported by the project "Development of System and Technology for Advanced Measurement and Analysis" of Japan Science and Technology Agency (JST).

## REFERENCES

1. A. Momose, S. Kawamoto, I. Koyama, Y. Hamaishi, K. Takai, and Y. Suzuki, "Demonstration of X-ray Talbot interferometry," *Jpn. J. Appl. Phys.* **42**, L866-L868 (2003).
2. T. Weitkamp, B. Nöhammer, A. Diaz, and C. David, "X-ray wavefront analysis and optics characterization with a grating interferometer," *Appl. Phys. Lett.* **86**, 054101 (2005).
3. T. Weitkamp, A. Daiz, C. David, F. Pfeiffer, M. Stampanoni, P. Cloetens, and E. Ziegler, "X-ray phase imaging with a grating interferometer," *Opt. Express* **13**, 6296-6304 (2005).
4. A. Momose, W. Yashiro, Y. Takeda, Y. Suzuki, and T. Hattori, "Phase tomography by X-ray Talbot interferometry for biological imaging," *Jpn. J. Appl. Phys.* **45**, 5254-5262 (2006).
5. S. Yokozeki and T. Suzuki, "Shearing interferometer using the grating as the beam splitter," *Appl. Opt.* **10**, 1575-1580 (1971).
6. A. W. Lohmann and D. E. Silva, "An interferometer based on the Talbot effect," *Opt. Commun.* **2**, 413-415 (1971).
7. A. Momose, S. Kawamoto, I. Koyama and Y. Suzuki, "Phase tomography using an X-ray Talbot interferometer," *SPIE Proc.* Vol. 5535, 352-360 (2004).
8. M. Matsumoto, K. Takiguchi, M. Tanaka, Y. Hunabiki, H. Takeda, A. Momose, Y. Utsumi, and T. Hattori, "Fabrication of diffraction grating for X-ray Talbot interferometer," *High Aspect Ratio Micro Structure Technology Workshop* (2005) pp.22-23.
9. J. P. Guigay, "On Fresnel diffraction by one-dimensional periodic object, with application to structure determination of phase objects," *Opt. Acta* **18**, 677-682 (1971).
10. K. A. Stetson and W. R. Brohinsky, "Electrooptic holography and its application to hologram interferometry," *Appl. Opt.* **24** 3631-3637 (1985).
11. G. W. Faris and R. L. Byer, "Three-dimensional beam-deflection optical tomography of a supersonic jet," *Appl. Opt.* **27** 5202-5212 (1988).
12. F. Pfeiffer, T. Weitkamp, O. Buck, and C. David, "Phase retrieval and differential phase-contrast imaging with low-brilliance X-ray sources," *Nature Phys.* **2**, 258-261 (2006).

# X-ray Phase Microtomography by Single Transmission Grating

Yoshihiro Takeda<sup>1</sup>, Wataru Yashiro<sup>2</sup>, Yoshio Suzuki<sup>3</sup> and Atsushi Momose<sup>2</sup>

<sup>1</sup>*Graduate School of Pure and Applied Sciences, University of Tsukuba,  
1-1-1 Tennodai, Tsukuba, Ibaraki 305-8573, Japan*

<sup>2</sup>*Department of Advanced Materials, Graduate School of Frontier Sciences, The University of Tokyo,  
5-1-5 Kashiwanoha, Kashiwa, Chiba 277-8561, Japan*

<sup>3</sup>*Japan Synchrotron Radiation Research Institute, SPring-8,  
1-1-1 Kouto, Sayo-cho, Sayo-gun, Hyogo 679-5198, Japan*

**Abstract.** A preliminary experiment of X-ray phase microtomography by a single phase grating is reported. A phase grating was placed behind an object and illuminated by spatially coherent X-rays. At a specific distance from the grating, a periodic intensity pattern caused by the fractional Talbot effect was recorded with a high spatial-resolution image detector. A differential phase map related to the object was retrieved from the deformation in the periodic intensity pattern on the basis of the fringe scanning method. Phase tomograms of a piece of polymer blend were reconstructed and a phase-separation structure in the blend was successfully resolved.

**Keywords:** Phase, Tomography, Interferometer, Imaging, Grating

**PACS:** 07.05.Pj, 07.85.Tt, 41.50.+h, 42.25.Hz, 42.30.-d, 42.30.Rx, 42.30.Wb

## INTRODUCTION

Because of the penetrating power of X-rays, X-ray absorption imaging makes it possible to observe internal structures of objects nondestructively. However, it is difficult to depict weakly absorbing structures in an object consisting of light elements. When X-rays pass through the object, however, quite a large phase shift occurs. Therefore X-ray phase imaging that measures the phase distribution of the X-rays, can realize high sensitive internal observation nondestructively.

Some methods for X-ray phase imaging was proposed in the middle of 1990s [1-3]. Recently, new X-ray interferometers consisting of X-ray gratings have been proposed and demonstrated [4-8]. The X-ray Talbot effect is used in the interferometers. When a grating is illuminated by spatially coherent X-rays, a periodic intensity pattern appears at a specific distance from the grating. In the X-ray Talbot interferometer [5], an absorption grating is overlaid on the periodic intensity pattern and generated moiré fringes are recorded. The pitch of the absorption gratings is made to be smaller than or comparable to the spatial coherence length of the incident X-rays. At the same time, it is required that the absorption grating is sufficiently thick to absorb the X-rays. This implies that a grating with a high aspect is required, but the fabrication of such a grating is not straightforward. On the other hand, the thickness of an X-ray phase grating can be much smaller than that of an absorption grating. Therefore it is comparatively easy to fabricate X-ray phase gratings. We propose a new method for X-ray phase imaging by a single phase grating that measures the periodic intensity pattern caused by the fractional Talbot effect with a high spatial-resolution detector instead of placing an amplitude grating on it.

## PRINCIPLE

Figure 1 shows the experimental set up of the proposed method. A phase grating with a pitch  $d$  is placed on the  $x$ - $y$  plane ( $z = 0$ ) so that the grooves of the grating are parallel to the  $y$  axis. When the phase grating is illuminated by

CP879, *Synchrotron Radiation Instrumentation: Ninth International Conference*,  
edited by Jae-Young Choi and Seungyu Rah

© 2007 American Institute of Physics 978-0-7354-0373-4/07/\$23.00

spatially coherent X-rays, a periodic intensity pattern appears at the downstream of the grating. Its intensity distribution  $I(x,y,z)$  is written by

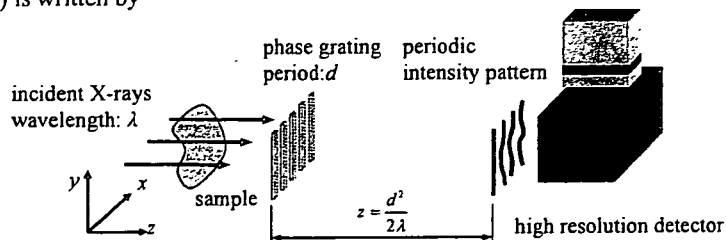


FIGURE 1. Experimental set up of the proposed technique.

$$I(x, y, z) = \sum_n b_n(z) \exp\left(2\pi i \frac{n}{d} x\right) \quad (1)$$

where  $b_n(z)$  is the  $n$ th Fourier coefficient which depends on the complex transmission function of the phase grating. For a phase grating with a transmission function  $T(x,y)=\exp[i\phi(x,y)]$ , the periodic intensity pattern at  $z = d^2/2\lambda$  is given by [9]

$$I\left(x, y, \frac{d^2}{2\lambda}\right) = 1 + \sin\left[\phi(x, y) - \phi\left(x + \frac{d}{2}, y\right)\right] \quad (2)$$

In the case of a  $\pi/2$  grating, the visibility of the pattern reaches 100% at  $z = d^2/2\lambda$ .

If an object with a phase shift  $\Phi(x,y)$  is put in front of the grating,  $I(x,y,z)$  is given by

$$I(x, y, z) = \sum_n b_n(z) \exp\left(2\pi i \frac{n}{d} \left[x - \frac{\lambda z}{2\pi} \frac{\partial \Phi(x, y)}{\partial x}\right]\right) \quad (3)$$

which indicates that the periodic intensity pattern is distorted by the object. A differential phase map  $\partial\Phi(x,y)/\partial x$  can be retrieved by the Fourier transform method or the fringe scanning method from the deformed periodic intensity pattern. By the Fourier transform method, the spatial resolution of the retrieved image is limited by the pitch of carrier fringes; that is, the period of the pattern in this case. On the other hand, the fringe scanning method has no limit with respect to the period in principle, and therefore we adopted the fringe scanning methods.

When the phase grating is displaced by the distance  $kd/M$  along the  $x$  direction, where  $k$  is an integer, the intensity distribution is given by

$$I_k(x, y, z) = \sum_n b_n(z) \exp\left(2\pi i \frac{n}{d} \left[x - \frac{\lambda z}{2\pi} \frac{\partial \Phi(x, y)}{\partial x} + \frac{d}{M} k\right]\right) \quad (4)$$

In the fringe scanning method, the fringe of a sinusoidal profile is normally assumed. Higher orders ( $n \geq 2$ ) in Eq. (4) are therefore the sources of error. However, by adequately selecting a large number for  $M$ , the error induced by the harmonics can be reduced [10]. We used 5-step fringe scan since the lowest order that causes error is 9th [7]. Because the magnitudes of such high orders are normally negligible, one can use a relation

$$2\pi \frac{n}{d} \left[ x - \frac{\lambda z}{2\pi} \frac{\partial \Phi(x, y)}{\partial x} \right] \approx \arg \left( \frac{\sum_{k=1}^5 I_k(x, y, z) \sin\left(2\pi \frac{k}{5}\right)}{\sum_{k=1}^5 I_k(x, y, z) \cos\left(2\pi \frac{k}{5}\right)} \right) \quad (5)$$

to calculate a differential phase map  $\partial\Phi(x,y)/\partial x$ . An X-ray phase map is obtained through operations of unwrapping and integration on the differential phase map. A phase tomogram can be reconstructed from multiple phase maps measured at various angular positions of the sample rotation.

## EXPERIMENT

The experiment was performed at BL20XU of SPring-8. X-rays emitted from an undulator was monochromatized to 17.7keV by a Si double-crystal monochromator. We used a phase grating with a gold pattern 8  $\mu\text{m}$  in pitch and 2  $\mu\text{m}$  in height fabricated by UV lithography and electro-plating. The pattern height corresponded to the amount for a  $\pi/2$  phase shift. We used a CCD camera with a phosphor screen and a coupling lens. The effective pixel size was 1.0  $\mu\text{m}$  and the field of view was about 1.3 mm  $\times$  1.0 mm. The camera was placed at  $z = d^2/2\lambda$  and generated periodic intensity pattern was measured with it. In front of the grating, a piece of polystyrene (PS) / poly (methyl methacrylate) (PMMA) polymer blend was put as a sample. The sample had phase separation structures consisting of PS-rich phase and PMMA-rich phase. Figure 2(a) shows a periodic intensity pattern obtained by an exposure of 1.5 seconds. An enlarged image of the area indicated with broken lines in Fig. 2(a) is shown in Fig. 2(b), where the distortion of fringes is clearly seen. Five distorted patterns were measured by displacing the phase grating along the  $x$  direction by a one-fifth of the pitch. A differential phase map was calculated from the patterns, as shown in Fig. 2(c).

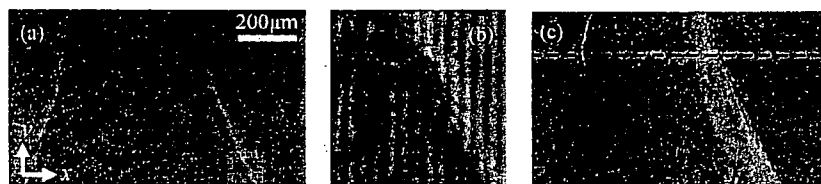


**FIGURE 2.** Distorted intensity pattern caused by a piece of polymer blend and calculated differential phase map. A close-up image of the region indicated by broken-line square in (a) is shown in (b). (c) is the differential phase map calculated on the basis of the fringe scanning method.

The sample was rotated in a 0.72-degree step over 180 degrees and 250 phase maps were obtained. Figure 3(a) shows a reconstructed phase tomogram at the position of the broken line in Fig. 2(c), and Fig. 3(b) shows a three-dimensional rendering view. The pixel values in reconstructed phase tomogram indicate the refractive index difference between the object and the surrounding air. The refractive index difference between the PS-rich phase and air was  $7.5 \times 10^{-7}$ , and between PMMA-rich phase and air was  $8.5 \times 10^{-7}$ . The detection limit of the refractive index deviation was evaluated to be  $1 \times 10^{-8}$  from the standard deviation of refractive index in the PMMA-rich phase. The spatial resolution in the phase tomogram was evaluated to be 7.5  $\mu\text{m}$  by the FWHM of differential profile across the boundary between the PS-rich and PMMA-rich phases.

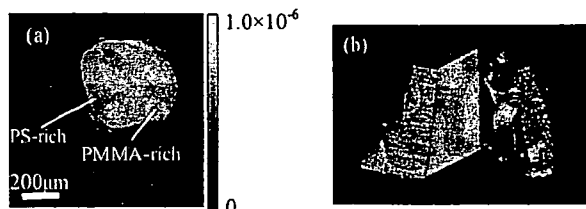


**FIGURE 3.** Reconstructed phase tomogram of a piece of polymer blend; (a) one of axial sections and (b) a three-dimensional rendering view, where the PS-rich region in the right-side part has been made transparent

## DISCUSSION

The detection limit of the refractive index deviation by this technique was worse than that of other techniques [7, 11]. The visibility of the measured periodic intensity pattern was only 8%, which might reflect on the result. The low visibility is considered to be due to the MTF of the detector. Using a detector with a better MTF will raise the visibility of measured pattern and therefore improve the sensitivity to refractive index deviation. If a phase grating with a period larger than that used in this study can be used within the permitted range determined by the spatial coherency, the sensitivity to refractive index deviation will be improved as well.

The spatial resolution of the fringe scanning method is limited by the pixel size in principle. Although presented result exceeded the limit of the sampling theorem in the case of using the Fourier-transform method, the resultant value  $7.5 \mu\text{m}$  was much worse than the pixel size of the image detector used. However, this result was predicted because the edge-contrast as seen in Fig. 2 caused by Fresnel diffraction is unavoidable. The amount of the blur (or the thickness of the edge contrast) is estimated to be  $\sqrt{\lambda z} = 5.6 \mu\text{m}$  in this case. When the object can be placed downstream of the grating, this blur will be reduced. However, it should be noted that the sensitivity is proportional to distance between the object and the detector, and therefore one has to compromise the decrease in sensitivity in this case. The fractional Talbot effect occurs when the phase grating is illuminated by spherical X-rays. Therefore, another approach for reducing the blur due to Fresnel diffraction is found by combining this method with X-ray imaging microscopy. Provided that an image detector of a wide field of view compatible with a small pixel size in the future, the presented technique would be an approach for attaching a phase-contrast mode in a simple way. In addition, we consider that the combination with an X-ray imaging microscope is an important future direction of the presented method.

## CONCLUSION

X-ray phase microtomography with a single phase grating was performed at BL20XU of SPring-8. An Au phase grating was placed behind an object and illuminated by spatially coherent X-rays. Periodic intensity pattern caused by the fractional Talbot effect was measured by a high resolution image detector. A differential phase map was retrieved by the fringe scanning method and phase tomograms were reconstructed. The combination with X-ray microscopy will be a next step, providing a new type differential phase microscopy, with which phase nanotomography would be attainable.

## ACKNOWLEDGEMENT

The experiment using synchrotron radiation was performed under the approval of SPring-8 committee 2006A1237-NM-np. This study was financially supported by the project "Development of System and Technology for Advanced Measurement and Analysis" of Japan Science and Technology Agency (JST).

## REFERENCES

1. A. Momose, *Nucl. Instrum. Methods* **352**, 622-628(1995)
2. T. J. Davis, D. Gao, T. E. Gureyev, A. W. Stevenson and S. W. Wilkins: *Nature* **373**, 595-598(1995)
3. A. Snigirev, I. Snigireva, V. Kohn, S. Kuznitsiv and I. Schelov, *Rev. Sci. Instrum.* **66**, 5486-5492 (1995)
4. C. David, B. Nöhammer, H. H. Solak and E. Ziegler: *Appl. Phys. Lett.* **81**, 3287-3289(2002)
5. A. Momose, S. Kawamoto, I. Koyama, Y. Hamaishi, K. Takai and Y. Suzuki: *Jpn. J. Appl. Phys.* **42**, L866-L868(2003)
6. T. Weitkamp, B. Nöhammer, A. Diaz, C. David, F. Pfeiffer, M. Stamparoni, P. Cloetens and E. Ziegler: *Appl. Phys. Lett.* **86**, 054101(2005).
7. A. Momose, S. Kawamoto, I. Koyama and Y. Suzuki, *SPIE Proc.* **5535**, 352-360 (2004)
8. E. Pfeiffer, T. Weitkamp, O. Buck and C. David, *Nature Phys.* **2**, 258-261(2006)
9. J. P. Guigay: *Opt. Acta* **18**, 677-682(1971)
10. K. A. Stetson and W. R. Brohinsky: *Appl. Opt.* **24**, 3631-3637(1985)
11. A. Momose, A. Fujii, H. Kadowaki and H. Jinnai: *Macromolecules* **38**, 7197-7200(2005)

# Phase Tomography Using X-ray Talbot Interferometer

A. Momose,<sup>1</sup> W. Yashiro,<sup>1</sup> Y. Takeda,<sup>2</sup> M. Moritake,<sup>1</sup>  
K. Uesugi,<sup>3</sup> Y. Suzuki,<sup>3</sup> and T. Hattori<sup>4</sup>

<sup>1</sup>*Graduate School of Frontier Sciences, The University of Tokyo,  
5-1-5 Kashiwanoha, Kashiwa, Chiba 277-8561, Japan*

<sup>2</sup>*Graduate School of Pure and Applied Sciences, University of Tsukuba,  
1-1-1 Tennodai, Tsukuba, Ibaraki 305-8573, Japan*

<sup>3</sup>*SPring-8/JASRI, 1-1-1 Kouto, Mikazuki, Hyogo 679-5198, Japan*

<sup>4</sup>*Laboratory of Advanced Science and Technology for Industry, University of Hyogo,  
3-1-2 Kouto, Kamigori, Hyogo 678-1205, Japan*

**Abstract.** A biological tomography result obtained with an X-ray Talbot interferometer is reported. An X-ray Talbot interferometer was constructed using an amplitude grating fabricated by X-ray lithography at the LIGA beamline of NewSUBARU and gold electroplating. The pitch and pattern thickness of the grating were 8  $\mu\text{m}$  and 30  $\mu\text{m}$ , respectively. The effective area was 20  $\times$  20  $\text{mm}^2$ , which was entirely illuminated with a wide beam available at the medium-length beamline 20B2 of SPring-8, allowing the acquisition of a three-dimensional tomogram of almost the whole body of a fish. The resulting image obtained with 17.7 keV X-rays revealed organs with bones in the same view.

**Keywords:** Tomography, Phase, Talbot effect, Talbot interferometer, Grating, High aspect ratio.

**PACS:** 07.05.Pj, 07.85.Tt, 41.50.+h, 42.25.Hz, 42.30.-d, 42.30.Wb,

## INTRODUCTION

Recently, X-ray transmission gratings have been implemented in novel phase-sensitive X-ray imaging [1-6]. Differential phase contrast can be generated by aligning two transmission gratings on an optical axis with a specific separation determined by the pitch of the gratings and X-ray wavelength. The first grating generates self-images that exhibit periodical intensity patterns corresponding to the transmission function of the grating. The self-images are induced by Fresnel diffraction by the grating, which is known as the fractional Talbot effect. When a phase object is placed in the path of X-rays, X-ray refraction at the phase object is reflected on the deformation of the self-images. The second grating, which is of the amplitude type with a pitch almost the same as the average period of a self-image and is placed at the position of the self-image, generates a moiré pattern by superposition with the deformed self-image. This system is known as a Talbot interferometer [7,8].

Because of its use of grating optics, Talbot interferometry has many advantages over other phase-sensitive X-ray imaging methods. One advantage is that the setting up of a Talbot interferometer is easy because gratings can be aligned with an accuracy corresponding to their pitch, which is set to be comparable to the X-ray spatial coherence length typically on the micrometer order. Another advantage is that a cone beam with a broad energy bandwidth (approx.  $E/\Delta E > 10$ ) can be used. In addition, it should be emphasized that the quantitative measurement of a differential phase image is feasible, enabling phase tomography.

In this paper, we describe a biological imaging result obtained by phase tomography using the X-ray Talbot interferometer at SPring-8. An amplitude grating 8  $\mu\text{m}$  in pitch and 30  $\mu\text{m}$  in thickness was fabricated by means of X-ray lithography and gold electroplating. Its effective area was 20  $\times$  20  $\text{mm}^2$ , which was covered with the wide beam of the beamline 20B2.

CP879, *Synchrotron Radiation Instrumentation: Ninth International Conference*,  
edited by Jae-Young Choi and Seungyu Rah

© 2007 American Institute of Physics 978-0-7354-0373-4/07/\$23.00



## X-RAY TALBOT INTERFEROMETER

Figure 1 shows a calculated X-ray intensity downstream from a  $\pi/2$  phase grating under plane-wave illumination of X-rays of wavelength  $\lambda$ . The spatial coherence length of the X-rays at the grating was assumed to be almost  $3d$ , where  $d$  is the pitch of the grating. At the positions given by  $m\lambda/4d^2$ , where  $m$  is an integer other than those which are multiples of four, rectangular periodic patterns (self-images) of period  $d$  are formed in a process known as the fractional Talbot effect. The visibility of the self-images decreases along the optical axis owing to the finite spatial coherence length.

When a phase object is placed in front of the grating, the self-images are deformed due to the refraction at the phase object. The amount of deformation is proportional to the distance the self-image from the grating. In a Talbot interferometer, an amplitude grating of period  $d$  is placed at the position of one of the self-images. Then, the deformation of the self-image is visualized as a moiré pattern induced by the superposition of the self-image and amplitude grating (see Fig. 2). In the experiment presented in this paper, we selected the position corresponding to  $m = 2$ , where the visibility of the self-image is at its maximum.

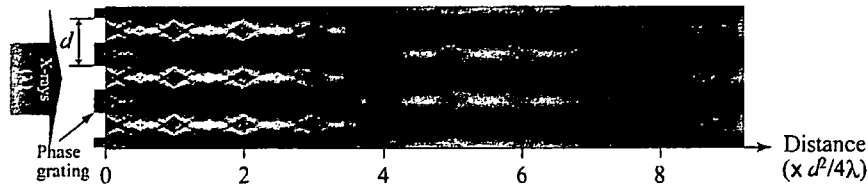


FIGURE 1. Calculation of intensity downstream of  $\pi/2$  phase grating induced by fractional X-ray Talbot effect under assumption of illumination of nearly plane-wave X-rays with spatial coherence length of  $3d$ .

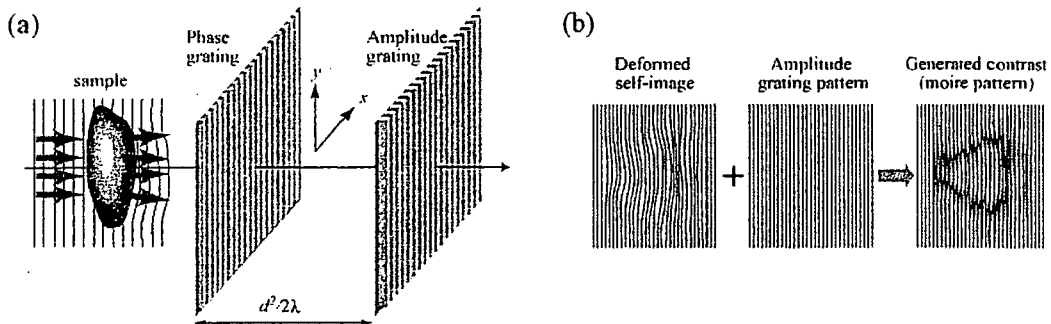


FIGURE 2. Configuration of Talbot interferometer (a) and schematic diagram (b) explaining moiré pattern generation.

The second grating used in the Talbot interferometer must, in principle, be of the amplitude type. The pattern of the grating should therefore be thick enough to absorb X-rays fully. Gold is a suitable material for this grating, considering its absorption coefficient and fabrication process. Nevertheless, a thickness much larger than  $10 \mu\text{m}$  is required. The pitch of the grating should be comparable to or smaller than the spatial coherence length of X-rays to induce the fractional Talbot effect. The spatial coherence length of hard X-rays from a storage ring is typically  $10 \mu\text{m}$ . Therefore, a pattern of high aspect ratio should be fabricated. We used such an amplitude grating fabricated by X-ray lithography and gold electroplating.

A  $30\text{-}\mu\text{m}$ -thick X-ray resist film (MAX001, Nagase ChemteX) was spin-coated on a  $200\text{-}\mu\text{m}$ -thick Si wafer with a  $0.25\text{-}\mu\text{m}$ -thick Ti layer. The beamline 11 of NewSUBARU, Japan, which is dedicated to Lithographic Galvanoformung Abformung (LIGA) fabrication, was used for X-ray exposure through an X-ray mask of an  $8\text{-}\mu\text{m}$ -pitch 1:1 line-and-space pattern. After developing, gold lines were formed by electroplating between resist lines, which were left after the electroplating to support the gold lines. The height of the gold lines was nearly  $30 \mu\text{m}$ , and the effective area of the grating was  $20 \times 20 \text{ mm}^2$ . The first grating was of the  $\pi/2$  phase type for  $20 \text{ keV}$  X-rays. The basic performance of the set of gratings was reported elsewhere [6]: the visibility of moiré fringes was about 80% at  $20 \text{ keV}$ ; it was greater than 30% at  $31 \text{ keV}$ .

A wide beam of the beamline 20B2 of SPring-8, Japan through a Si 111 double-crystal monochromator was used 206 m from a bending section, and the entire effective area of the gratings was illuminated by the beam. The spatial coherence length of the X-rays at the interferometer was calculated to be about 20  $\mu\text{m}$ .

A CCD camera (C4742-95HR, Hamamatsu Photonics) lens-coupled with a phosphor screen was used to record moiré fringes. Its effective pixel size was 11.8  $\mu\text{m} \times 11.8 \mu\text{m}$ . A cell filled with formalin was placed close to the upstream side of the phase grating, and a sample was immersed in formalin. For tomography, the sample was rotated about the vertical axis. The lines of the gratings were also aligned vertically (parallel to the  $y$ -axis in Fig. 2(a)), such that the refraction in the horizontal plane was sensed.

Quantitative measurement of the angular beam deflection induced by the refraction at the sample, that is, a differential phase image, was carried out by observing the change in moiré patterns with the displacement of the amplitude grating in the  $x$ -direction (see Fig. 2(a)). The step of the displacement was  $d/5$  and five moiré patterns were used to calculate a differential phase image using the fringe scanning method [9]. This measurement was repeated for every angular position of the sample rotation in tomography.

### PHASE TOMOGRAM

Figure 3(a) shows the result of the measurement of a differential phase image of a fish (*Hasemania nana*) 3 cm in length obtained with 17.7 keV X-rays. This image was calculated from five moiré patterns, one of which is shown in Fig. 3(b). The contribution of moiré fringes appearing in the background in Fig. 3(b), which was mainly due to the pitch mismatch between the amplitude grating and the self-image, was removed using the data obtained in the absence of the sample.

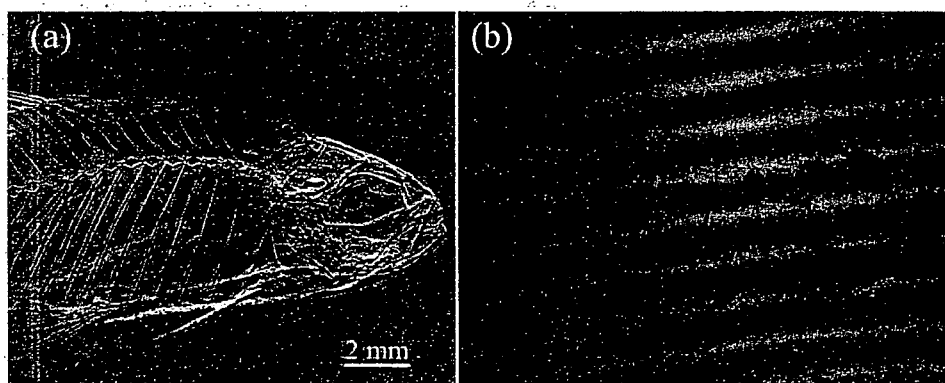


**FIGURE 3.** Differential phase image (a) of fish (*Hasemania nana*) calculated from a series of moiré patterns, one of which is shown in (b), recorded by fringe scanning. The X-ray energy was 17.7 keV. The vertical direction in these pictures corresponds to the  $x$ -direction in Fig. 2(a).

The angular step of the sample for phase tomography was  $0.36^\circ$ , and 500 differential phase images were recorded. The exposure time for obtaining a moiré image was 8.2 s. Before the tomographic reconstruction using the convolution-backprojection algorithm, each differential phase image was converted to a phase image through integration. Figure 4 shows sectional images generated using reconstructed three-dimensional data. Although artifacts remain because strong refractions at the bones and body surface could not be processed correctly within the assumption in the theory of X-ray Talbot interferometry that we used [2,9], organ structures are clearly revealed with bones in the same view, showing a wide dynamic range.

### CONCLUSION

Thus, X-ray Talbot interferometry exhibited an excellent sensitivity to soft structures. As for the spatial resolution, the pitch of the gratings gives a limit. Because a cone-beam is available with an X-ray Talbot interferometer, a next possible progress is in combining such an interferometer with a normal X-ray imaging microscope as an attachment for use in a phase-contrast mode. Another possibility of progress, with which X-ray Talbot interferometry will prove its full merit, is the development of an X-ray imaging apparatus for practical

applications such as medical diagnosis not only with synchrotron radiation sources but also with compact X-ray sources. For this purpose, we need to move to a higher-energy region, and the thickness and effective area of the amplitude grating should therefore be increased.

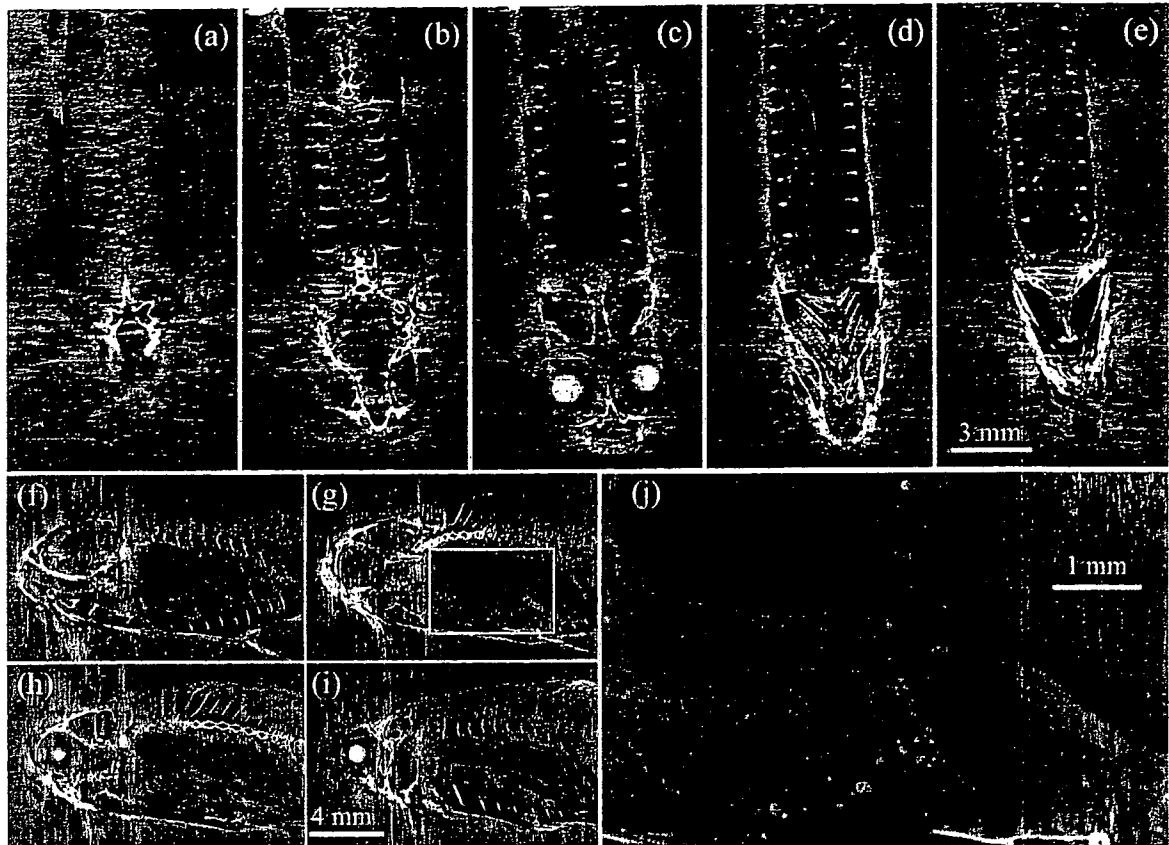


FIGURE 4. Phase tomograms of fish (*Hasemania nana*): coronal views (a)-(e) from back to stomach at 1.18 mm intervals and sagittal views (f)-(i) at 0.59 mm intervals. (j) is a magnified image of the area indicated by a rectangle in (g). Images map the refractive index difference from that of formalin ranging from  $-1 \times 10^{-7}$  to  $1 \times 10^{-7}$ .

## ACKNOWLEDGMENTS

The experiment using synchrotron radiation was performed under the approval of the SPring-8 committee 2006A1237-NM-np. This study was financially supported by the project "Development of System and Technology for Advanced Measurement and Analysis" of Japan Science and Technology Agency (JST).

## REFERENCES

1. C. David, B. Nöhammer, H. H. Solak, and E. Ziegler, *Appl. Phys. Lett.* **81**, 3287-3289 (2002).
2. A. Momose, S. Kawamoto, I. Koyama, Y. Hamaishi, K. Takai, and Y. Suzuki, *Jpn. J. Appl. Phys.* **42**, L866-L868 (2003).
3. T. Weitkamp, B. Nöhammer, A. Diaz, and C. David, *Appl. Phys. Lett.* **86**, 054101 (2005).
4. T. Weitkamp, A. Daiz, C. David, F. Pfeiffer, M. Stampanoni, P. Cloetens, and E. Ziegler, *Opt. Express* **13**, 6296-6304 (2005).
5. F. Pfeiffer, T. Weitkamp, O. Buck, and C. David, *Nature Phys.* **2**, 258-261 (2006).
6. A. Momose, W. Yashiro, Y. Takeda, Y. Suzuki, and T. Hattori, *Jpn. J. Appl. Phys.* **45**, 5254-5262 (2006).
7. S. Yokozeki and T. Suzuki, *Appl. Opt.* **10**, 1575-1580 (1971).
8. A. W. Lohmann and D. E. Silva, *Opt. Commun.* **2**, 413-415 (1971).
9. A. Momose, S. Kawamoto, I. Koyama, and Y. Suzuki, *SPIE Proc.* **5535**, 352-360 (2004).

## X-Ray Phase Imaging with Single Phase Grating

Yoshihiro TAKEDA, Wataru YASHIRO<sup>1</sup>, Yoshio SUZUKI<sup>2</sup>, Sadao AOKI, Tadashi HATTORI<sup>3</sup>, and Atsushi MOMOSE<sup>1</sup>

Graduate School of Pure and Applied Sciences, University of Tsukuba, 1-1-1 Tennodai, Tsukuba, Ibaraki 305-8573, Japan

<sup>1</sup>Department of Advanced Materials Science, Graduate School of Frontier Sciences, The University of Tokyo,

5-1-5 Kashiwanoha, Kashiwa, Chiba 277-8561, Japan

<sup>2</sup>Japan Synchrotron Radiation Research Institute, SPring-8, 1-1-1 Kouto, Sayo, Hyogo 679-5198, Japan

<sup>3</sup>Laboratory of Advanced Science and Technology for Industry, University of Hyogo, 3-1-2 Kouto, Kamigori, Hyogo 678-1205, Japan

(Received August 31, 2006; accepted November 1, 2006; published online January 12, 2007)

X-ray phase imaging with a single phase grating based on the fractional Talbot effect is described. A phase grating with an 8  $\mu\text{m}$  pitch was placed behind a weakly absorbing object and illuminated with partially coherent 17.7 keV X-rays. Intensity patterns downstream of the grating were recorded with a high-resolution image detector. By the fringe scanning method, an X-ray wavefront inclination by the object was obtained. Phase tomography was performed and the three-dimensional structure of a piece of a polymer blend was revealed with an 8  $\mu\text{m}$  spatial resolution and a 9  $\text{mg}/\text{cm}^3$  detection limit of density deviation. [DOI: 10.1143/JJAP.46.L89]

KEYWORDS: X-ray imaging, phase measurement, Talbot effect, tomography, X-ray interferometer

Because of the penetrating power of X-rays, X-ray absorption imaging makes it possible to observe internal structures of objects nondestructively. However, it is difficult to depict weakly absorbing structures of an object consisting of light elements. When X-rays pass through an object, however, a considerably large phase shift occurs. Therefore, X-ray phase imaging that measures the distribution of an X-ray phase shift enables us to observe internal structures with high sensitivity. For X-ray phase imaging, many approaches were proposed and demonstrated in the middle of 1990s.<sup>1–3)</sup>

Recently, X-ray phase imaging setups consisting of X-ray gratings have been reported.<sup>4–8)</sup> Because these setups do not use crystal optics, it is possible to perform X-ray phase imaging with polychromatic and/or spherical-wave X-rays. When a phase grating is illuminated with partially coherent plane-wave X-rays, clear periodic intensity patterns whose periods correspond to the pitch of the grating appear at specific distances from the grating (fractional Talbot effect).<sup>9–11)</sup> The pitch of the grating is chosen such that it is comparable to or smaller than the spatial coherence length of incident X-rays, usually below 10  $\mu\text{m}$ . In these methods, the second grating, which should be absorption type, is overlaid on an intensity pattern, and the appearing moiré fringes whose spacings are much larger than the period of the intensity pattern are measured easily with a normal X-ray image detector. When a phase object is placed in front of the first grating, X-ray refraction at the objects causes the deformation of the periodic intensity pattern and therefore of the moiré fringes.

Note that we can omit the absorption grating if we can resolve the intensity pattern downstream of the first grating directly with an image detector. The X-ray fractional Talbot effect has been observed with a charge coupled devices (CCD) coupled with a scintillator and a coupling lens or an X-ray film.<sup>4,5,12)</sup> For X-rays above 10 keV, the fabrication of an absorption grating is crucial because a pattern with an extremely high aspect ratio needs to be formed, which is not straightforward by normal lithographic techniques. Therefore, an approach that eliminates the use of an X-ray absorption grating and instead employs a high-spatial-resolution image detector is a good alternative. In addition,

this approach opens up a new possibility for X-ray phase-sensitive microscopy.

In this paper, we describe an experimental demonstration of X-ray phase imaging with a single phase grating and a high-spatial-resolution image detector.

Let us consider a phase grating with a pitch  $d$  placed on the  $xy$ -plane ( $z = 0$ ) so that the grooves of the grating are parallel to the  $y$ -axis. The complex transmission function of the grating  $T(x)$  is expressed by a Fourier series expansion as

$$T(x) = \sum_n a_n \exp\left(2\pi i \frac{n}{d} x\right), \quad (1)$$

where  $a_n$  is the  $n$ th Fourier coefficient. When the grating is illuminated with unit-amplitude plane-wave X-rays whose wavelength is  $\lambda$ , the complex amplitude  $E(x, y, z)$  of the X-rays downstream of the grating is also expressed by a Fourier series expansion as

$$\begin{aligned} E(x, y, z) &= \frac{1}{\sqrt{i\lambda z}} \int T(x_0) \exp\left[\frac{\pi i}{\lambda z} (x - x_0)^2\right] dx_0 \\ &= \sum_n b_n(z) \exp\left(2\pi i \frac{n}{d} x\right), \end{aligned} \quad (2)$$

with paraxial approximation,<sup>13)</sup> where

$$b_n(z) \equiv a_n \exp\left(-\pi i \lambda z \frac{n^2}{d^2}\right). \quad (3)$$

Equations (2) and (3) indicate that the Fourier coefficient  $b_n$  varies along the optical axis ( $z$ -axis). The intensity distribution  $I(x, y, z)$  is given by

$$\begin{aligned} I(x, y, z) &= |E(x, y, z)|^2 \\ &= \sum_n c_n(z) \exp\left(2\pi i \frac{n}{d} x\right), \end{aligned} \quad (4)$$

where

$$c_n(z) \equiv \sum_{n'} b_{n+n'}(z) b_{n'}^*(z). \quad (5)$$

At specific distances from the grating, clear periodic intensity patterns whose period is the same as that of the grating appear, as shown in Fig. 1, which is a calculated intensity distribution downstream of a  $\pi/2$  shift phase grating.